Supporting Information for

# Controlling Rotation of Two-Dimensional Material Flakes

Shuze Zhu[1]*, Pascal Pochet[2]*, Harley T. Johnson[1]*

[1]Department of Mechanical Science and Engineering, University of Illinois at Urbana-Champaign, Urbana, IL 61801, USA

[2]Laboratory of Atomistic Simulation (L_Sim), Univ. Grenoble Alpes & CEA 38054 Grenoble, FRANCE

Email of corresponding authors*:

Shuze Zhu (shuzezhu@illinois.edu)

Pascal Pochet (pascal.pochet@cea.fr )

Harley T. Johnson (htj@illinois.edu)

This supporting file contains the following:

1. MD relaxation process and characterization of rotation angle
2. Interfacial stacking of the atomistic structure
3. Interfacial lattice model set up
4. Moiré domain model set up
5. Comparison between interfacial lattice model and moiré domain model
6. Demonstration of general applicability
7. Energy maps
8. Calculating of $MoSe_2$/graphene system with experimental comparison
9. Evolving energy landscapes during growth

## 1. MD relaxation process and characterization of rotation angle

Figure S1(a) shows that a triangular flake of $MoS_2$ is placed on another layer of $MoS_2$ with AA stacking (also see Figure S2 for higher resolution). The lattice constant for $MoS_2$ is 0.319 nm. Periodic boundary conditions are applied in the x-y direction. Color coding of each atom type is shown in Figure S1(b), and used throughout this supporting document if not otherwise noted. Figure S1(c) and (d) show that before structural relaxation, the top layer is rigidly rotated by 1 degree and 6 degrees, respectively. Then structural relaxation is carried out using the conjugate gradient (CG) algorithm followed by Hessian-free truncated Newton algorithm until either the total energy change between successive iterations divided by the energy magnitude is less than or equal to $10^{-20}$ or the total force is less than $10^{-15}$ eVÅ$^{-1}$. The MD relaxation for graphene is carried out similarly.

When the structural relaxation is complete, for each interface atom of the top flake (e.g., S atom in the case of $MoS_2$), one is able to calculate the associated deformation gradient $F$ using the unrelaxed structure as the reference. Then the deformation gradient is decomposed into the right stretch tensor and rotation matrix $F = R\,U$. The local rotation of each interface atom can be calculated from the rotation matrix. Then the global rotation of the top flake is assumed to be the arithmetic average of all the local rotation.

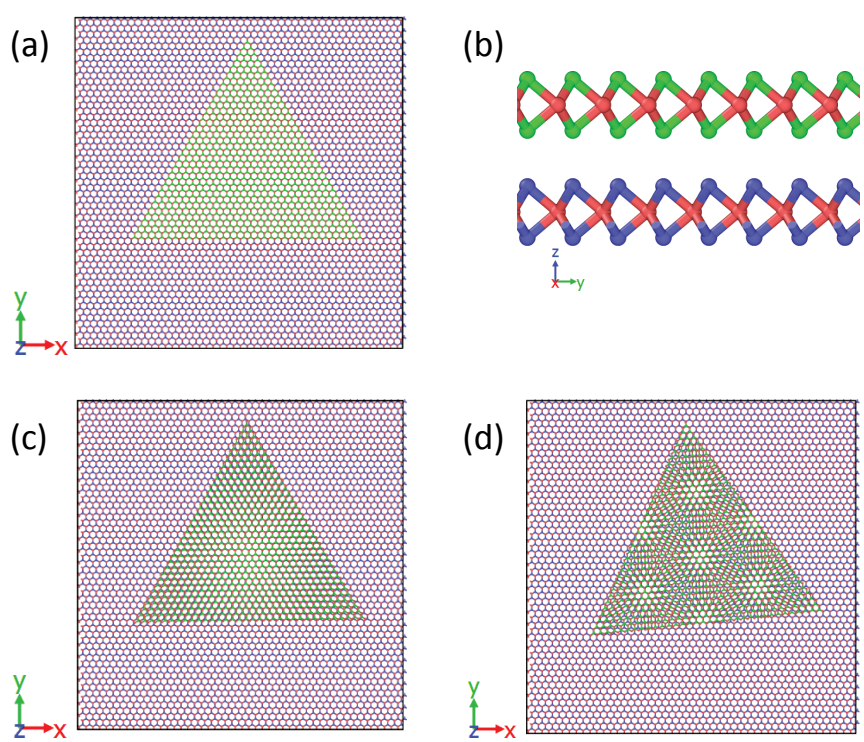


***Figure S1:*** *(a) Atomistic model with the top view. The bounding box denotes the periodical boundary conditions. (b) Side view of the bilayer structure in (a) showing the coloring scheme. (c) A rigid rotation of 1 degree is imposed counterclockwise on the top flake in (a) before structural relaxation. (d) A rigid rotation of 6 degree is imposed counterclockwise on the top flake in (a) before structural relaxation. The material system is bilayer $MoS_2$.*

## 2. Interfacial stacking of the atomistic structure

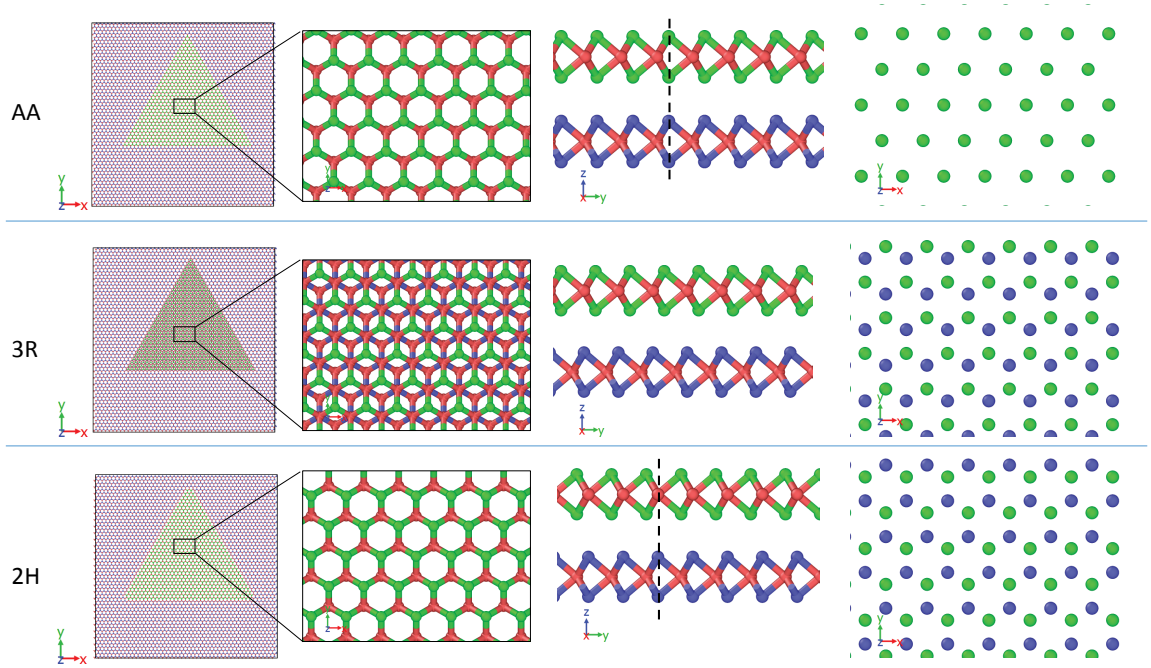


***Figure S2:*** *Each row shows for a specific stacking pattern, the associated interfacial stacking pattern. 3R and 2H share the same interfacial stacking as AB stacking, while AA stacking remains AA stacking at the interface. The material system is bilayer* $MoS_2$.

## 3. Interface lattice model set up

To calculate the structure-energy relationship in the interface lattice model, the interaction between the interface atoms (i.e., X atom and the X' atom in Figure 3(a) and Figure S3(a) for $MoS_2$) is described using a standard 12-6 potential

$$V(r) = 4 * \epsilon(\frac{s^{12}}{r^{12}} - \frac{s^6}{r^6})$$

Where $\epsilon = 1\ eV$, $d_0 = 0.339\ nm$ is the equilibrium distance of the above potential.

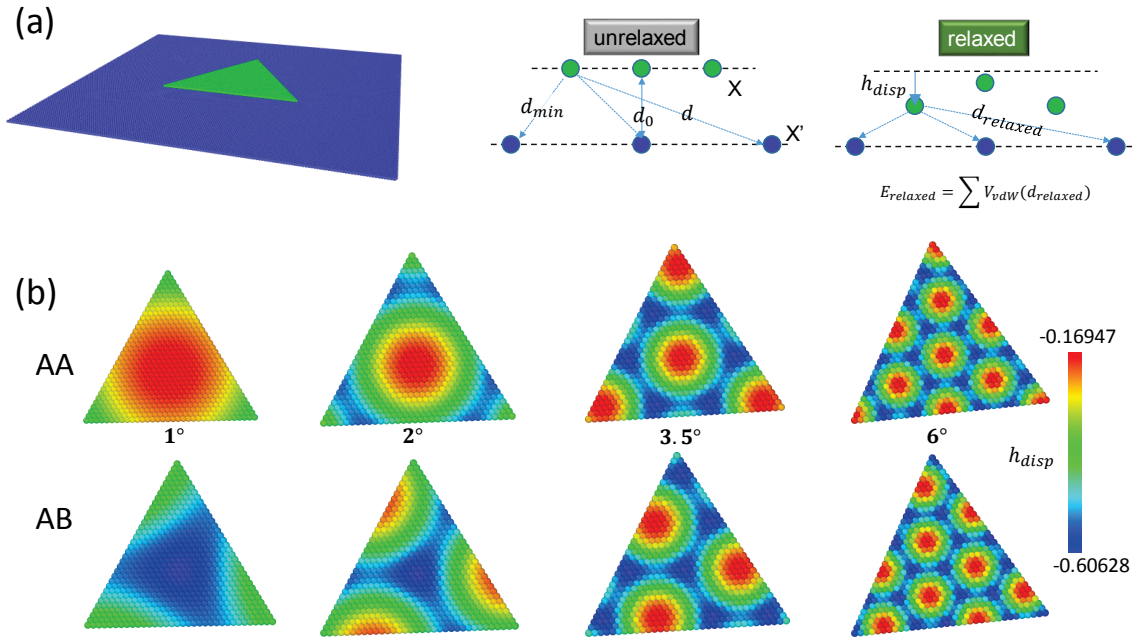


***Figure S3:*** *Applying interface lattice model to bilayer $MoS_2$. (a) We consider only the moiré patterns formed between the interfacial chalcogenide layers, which carry the first-order interlayer interactions. A square layer of chalcogenide atoms (X' layer in Figure 3(a)) supports a triangular layer of chalcogenide atoms (X layer in Figure 3(a)). An in-plane twist is applied on the top layer (the top X layer, shown in green). Further relaxation is performed using conjugate-gradient minimization on the total vdW energy of the X layer. Only out-of-plane displacements of the X atoms are permitted while the bottom X' atoms are fixed. (b) For the flake size same as in Figure 2, the height variation in the AA and AB stacking cases for a series of rotation angles. The unit of the color scale bar is Angstroms. This result is calculated from the interface lattice model using the parameters described above.*

## 4. Moiré domain model set up

The high energy domain and low energy domain are modeled as equal-radius circles tangential to each other. The coordinates of the center of these circles, and their diameter (related to the moire wavelength), as a function of rotation angle, can be determined following the framework established by Hermann, K. Journal of Physics-Condensed Matter 2012, 24, (31). (doi:10.1088/0953-8984/24/31/314210)

For example, in Figure S4(a)

$$\lambda(\theta) = \frac{(1+\delta)a}{\sqrt{2(1+\delta)[1-cos\theta]+\delta^2}}$$

where $\delta$ is the lattice mismatch strain and $\theta$ is the rotation angle.

Then $D_{high} = D_{low} = \frac{\lambda(\theta)}{\sqrt{3}}$

The total energy within the area of the triangle is calculated by summing up the energies of the evolving area of the circles within that triangle boundary (including partial circles that are cut by the boundary, and the transitional area) at a given flake rotation.

Without losing generality, we take the following dimensionless parameters for energies.

$$E_{high} = 1.5$$

$$E_{low} = 1$$

$$E_{transition} = 1.25$$

Thus, the total energy within the triangle is calculated as

$$E_{total} = \frac{A_{high} * E_{high} + A_{low} * E_{low} + \left(A_{total} - A_{high} - A_{low}\right) * E_{transition}}{A_{total}}$$

Where $A_{high}$ is the total area of the high energy circles within that triangle boundary (including partial circles that are cut by the boundary) at a given flake rotation. The $A_{low}$ is defined accordingly.

Figure S4(b) demonstrates a good agreement between the calculated location of centers of the circles with the interface lattice model.

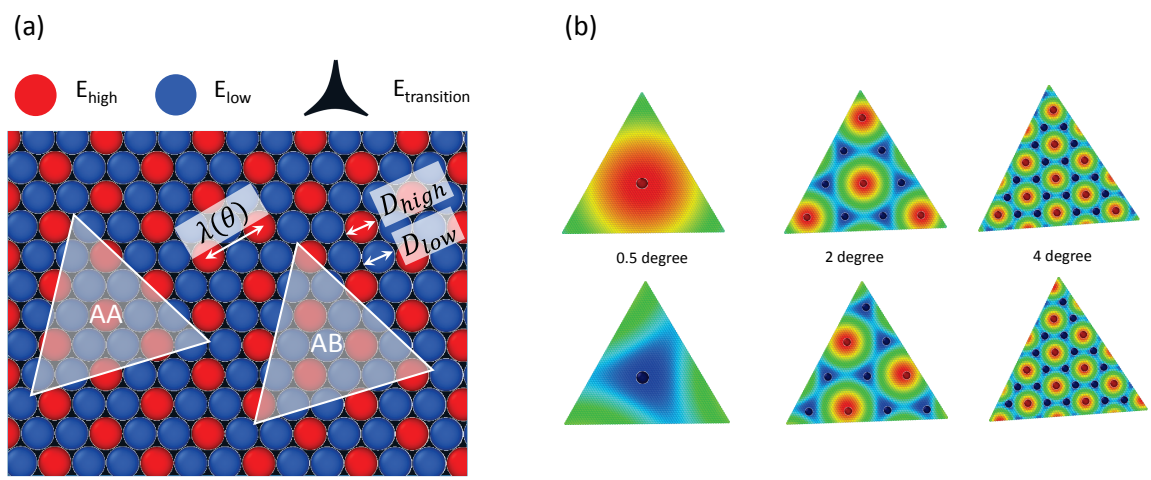


***Figure S4:*** *(a) Detailed schematic of the moiré domain model (MDM). Three types of energy domains are considered. (b) Good agreement between the geometry predicted in MDM model and ILM model, in terms of the centers of the high energy domain (red) and low energy domain (blue).*

## 5. Comparison between interfacial lattice model and moiré domain model

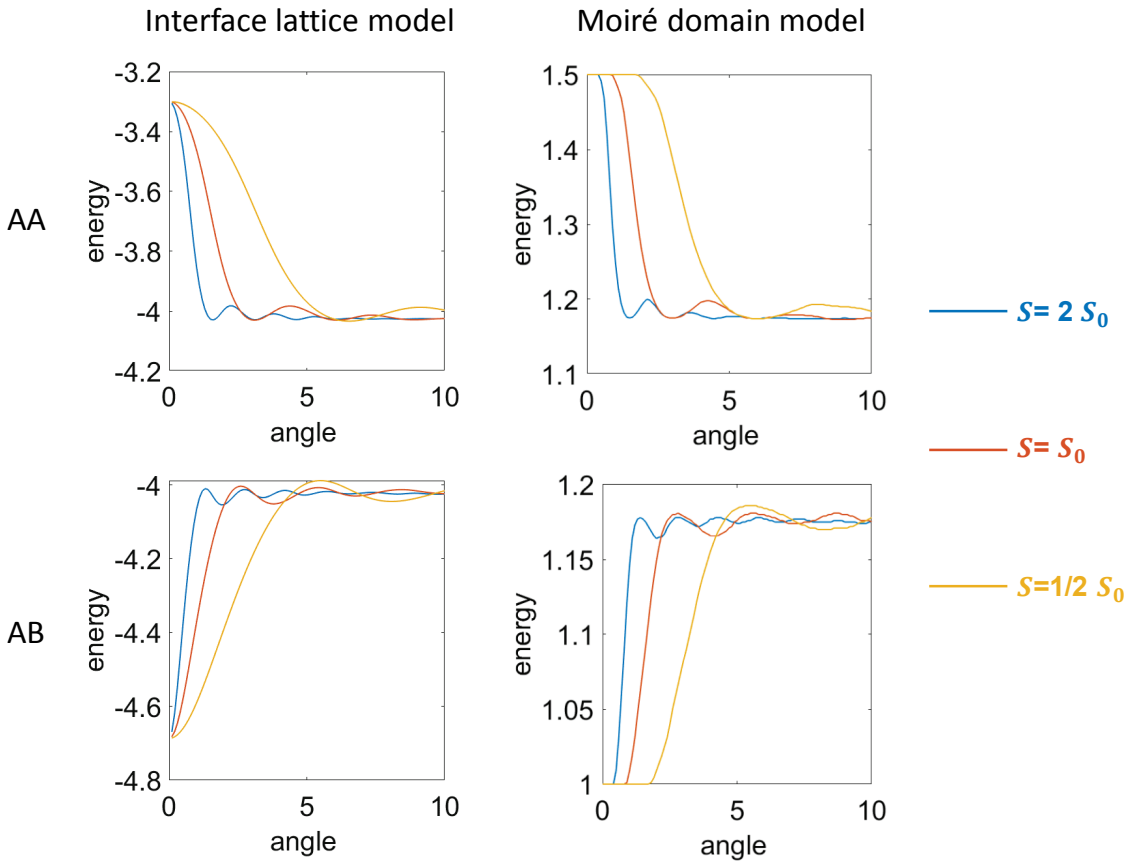


***Figure S5:*** *Comparison of energy-angle curves for $MoS_2$ between ILM calculation result and MDM.*

## 6. Demonstration of general applicability

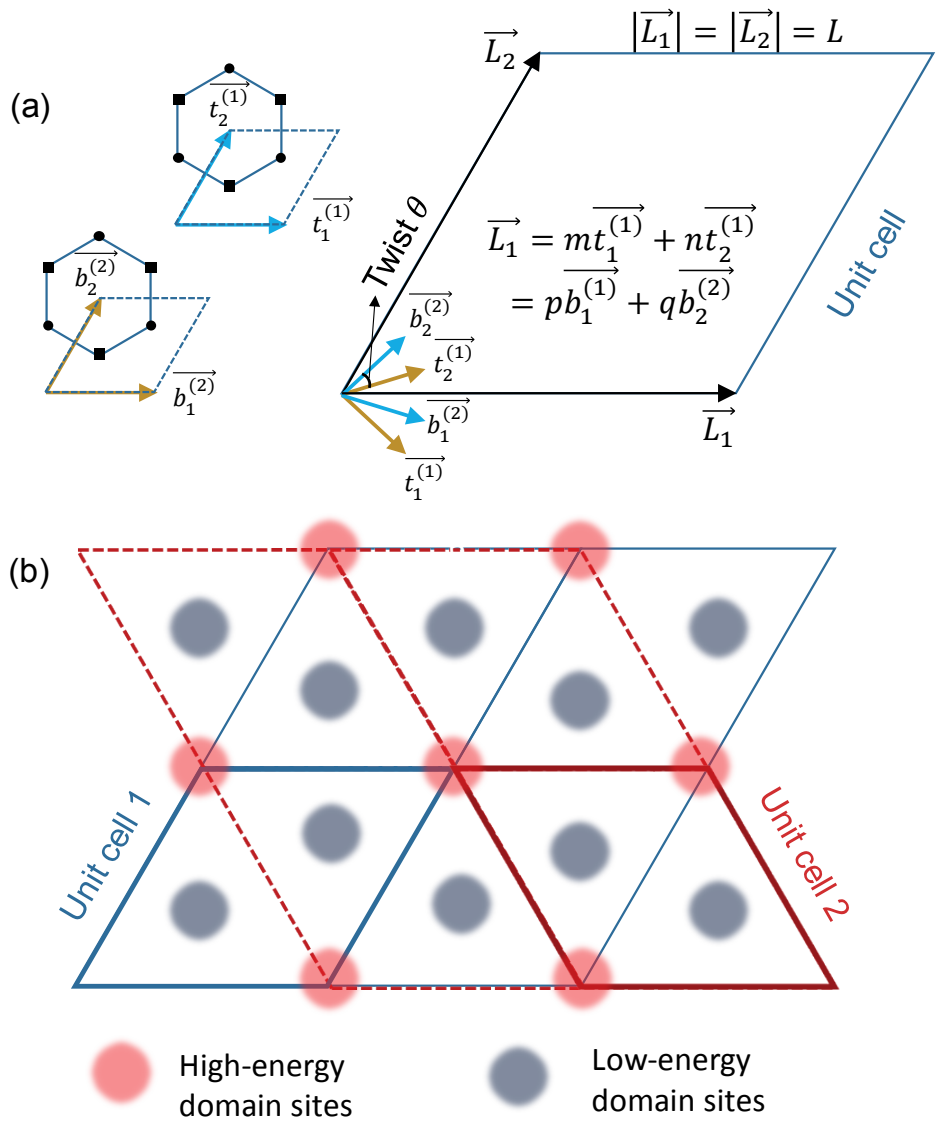


***Figure S6:*** *Origin of geometrical similarity in the moiré formed between 2 layers of 2D materials. (a) The moiré unit cell can be formed when the linear combination condition of lattice unit cell vectors from different layers can be met. This condition is necessary for common supercell vectors to be found in terms of each layer. The m, n, p, q are integers. The resulting moiré unit cell will also be a parallelogram with interior angles of 60 degrees or 120 degrees. (b) There are two applicable moiré unit cells. The overlapping of the supercell constructed from these two moiré unit cells allows us to further identify the translational periodical distribution of stacking domains. Required by the energy minimum principle, we can assign the majority of the sites as low-energy domain sites, which form a hexagonal lattice. The rest of the sites are assigned as high-energy domains and form a triangular lattice. Since the argument here is purely geometrical and energetic, the moiré domain analysis of the rotation of 2D material flakes is applicable generally in geometrically similar systems.*

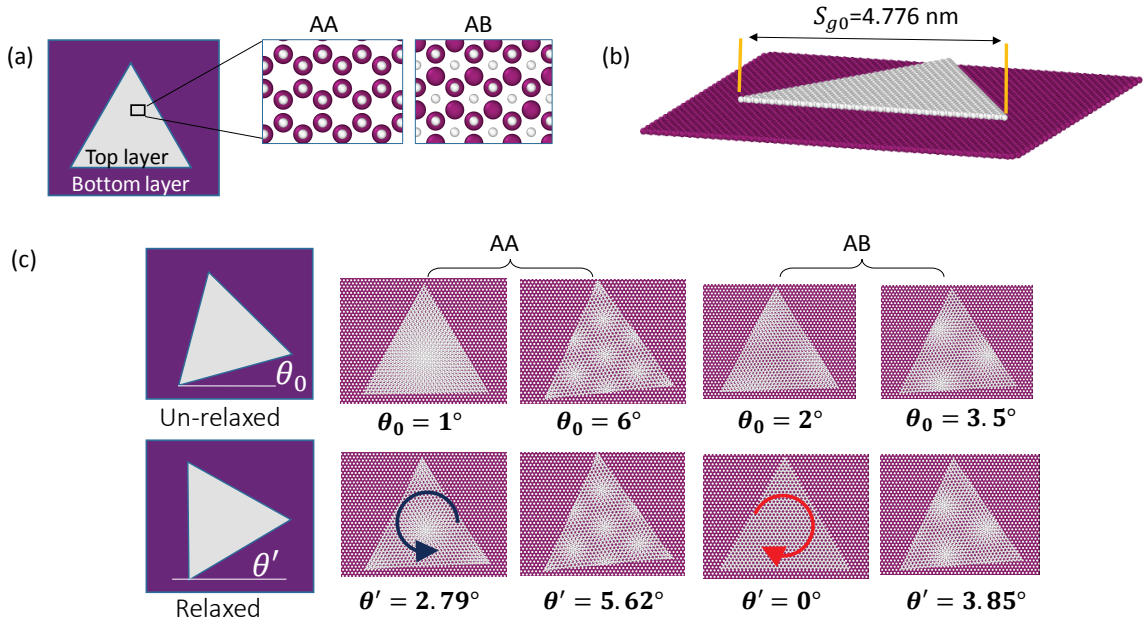


***Figure S7:*** *(a) Schematic showing the MD simulation model of bilayer graphene, in which a triangular top layer is placed on a large bottom layer. Two initial stacking patterns are studied. (b) Perspective view of the atomistic model of the bilayer graphene. The ratio of the simulated triangular flake size to its lattice constant is the same as that of $MoS_2$ in the preceding study, so we can compare a geometrically similar system (i.e., $S_{g0}/S_0$=lattice constant of graphene/lattice constant of $MoS_2$). (c) MD simulation results. The top row shows the initial stacked and rotated, unrelaxed configurations; the bottom row shows the relaxed configurations from MD simulations. Very much similar rotation behaviors with that of $MoS_2$ are observed, for geometrically similar 2D material systems where the ratio of the triangular flake size to the lattice constant is the same.*

The graphene simulation is using the AIREBO reactive force field (Stuart, S.; Tutein, A.; Harrison, J., A reactive potential for hydrocarbons with intermolecular interactions. Journal of Chemical Physics 2000, 112 (14), 6472-6486. https://doi.org/10.1063/1.481208)

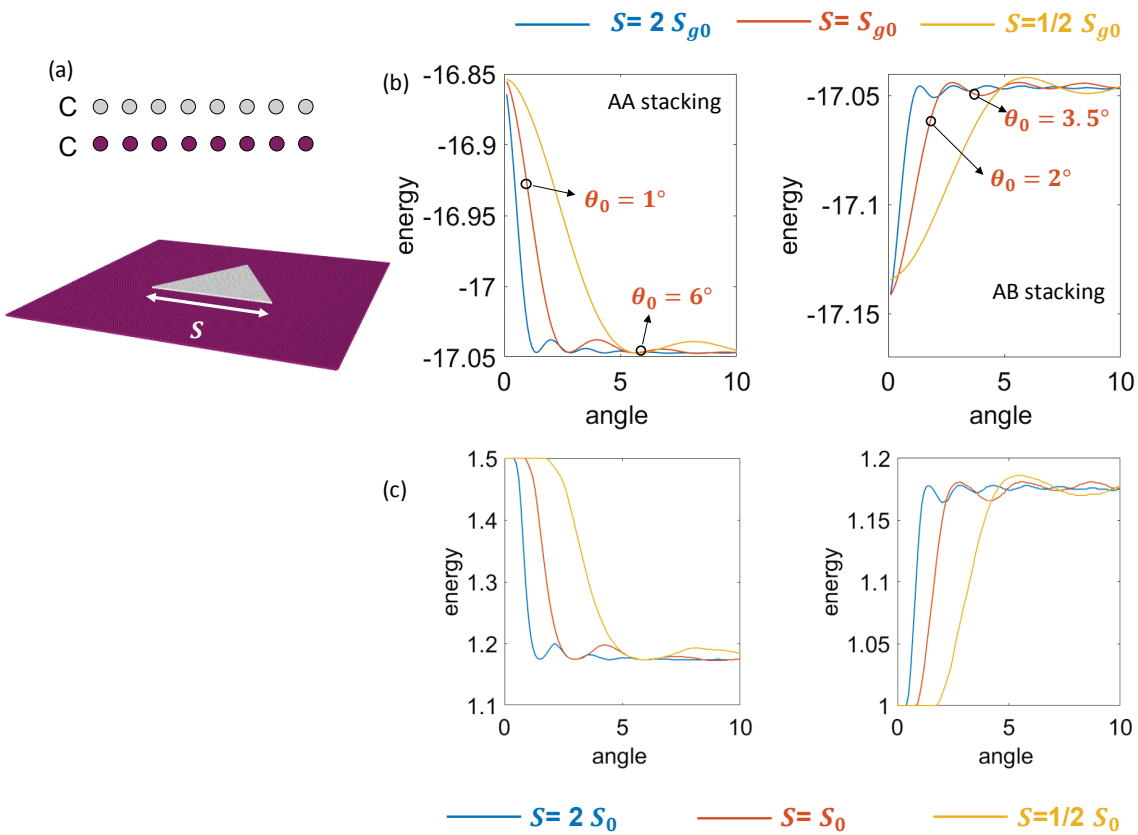


***Figure S8:*** *(a) Schematic showing the interface lattice model (ILM) for bilayer graphene, where only the atomic layers at the interface are considered. (b) Energy-angle curves from the ILM calculation, for three graphene flake sizes and two interface stacking variants. The labeled angles correspond to the MD simulation shown in Figure S7. (c) The general moiré domain model (MDM) result for the geometrically similar $MoS_2$ system calculated earlier (i.e., $S_{g0}/S_0$=lattice constant of graphene/lattice constant of $MoS_2$). The good agreement suggests that for geometrically similar different 2D material systems where the ratio of the triangular flake size to its lattice constant is the same, the rotation behavior will be, in general, the same.*

## 7. Energy maps

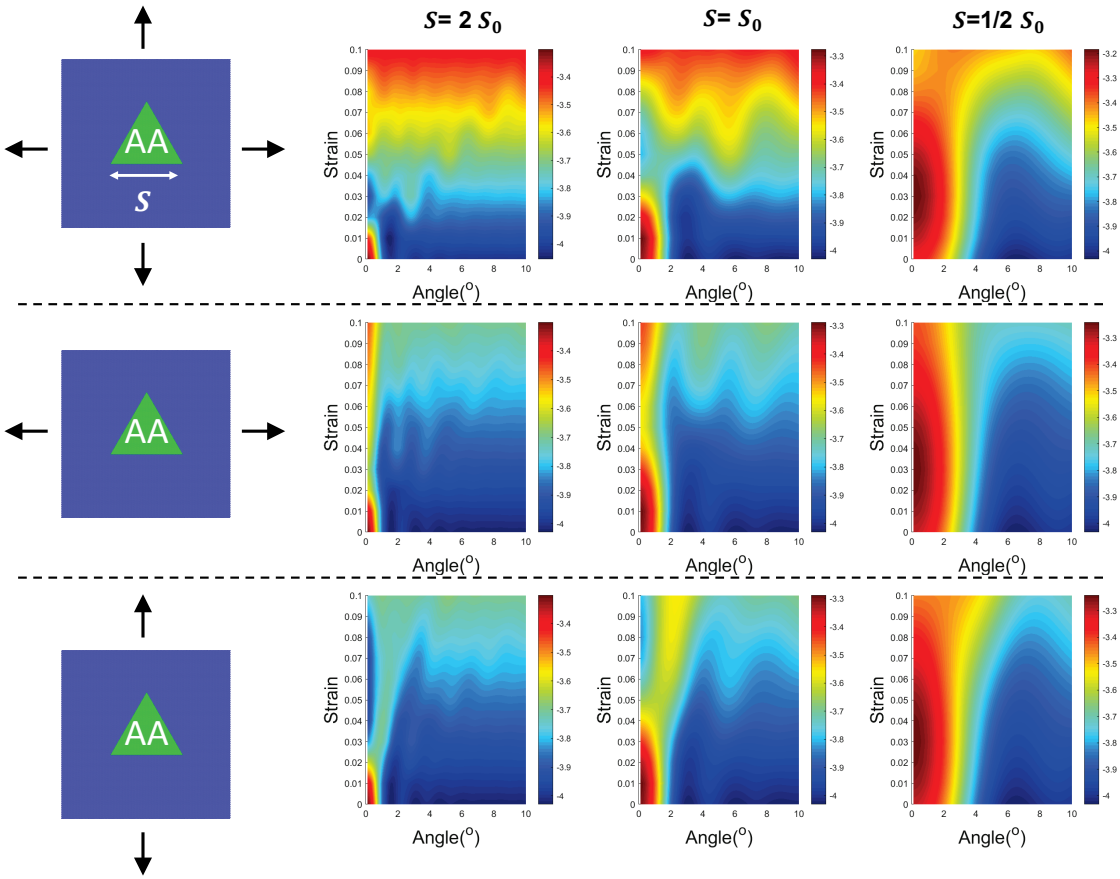


***Figure S9:*** *Energy maps in the space of strain and angle for three sizes. The top rows are for biaxial strain. The bottom two rows are for two uniaxial strain. The rotation center initial stacking is AA. Please note that this map is general for 2D material systems which share the same ratio of the triangular flake size to its lattice constant. See related discussion in main text.*

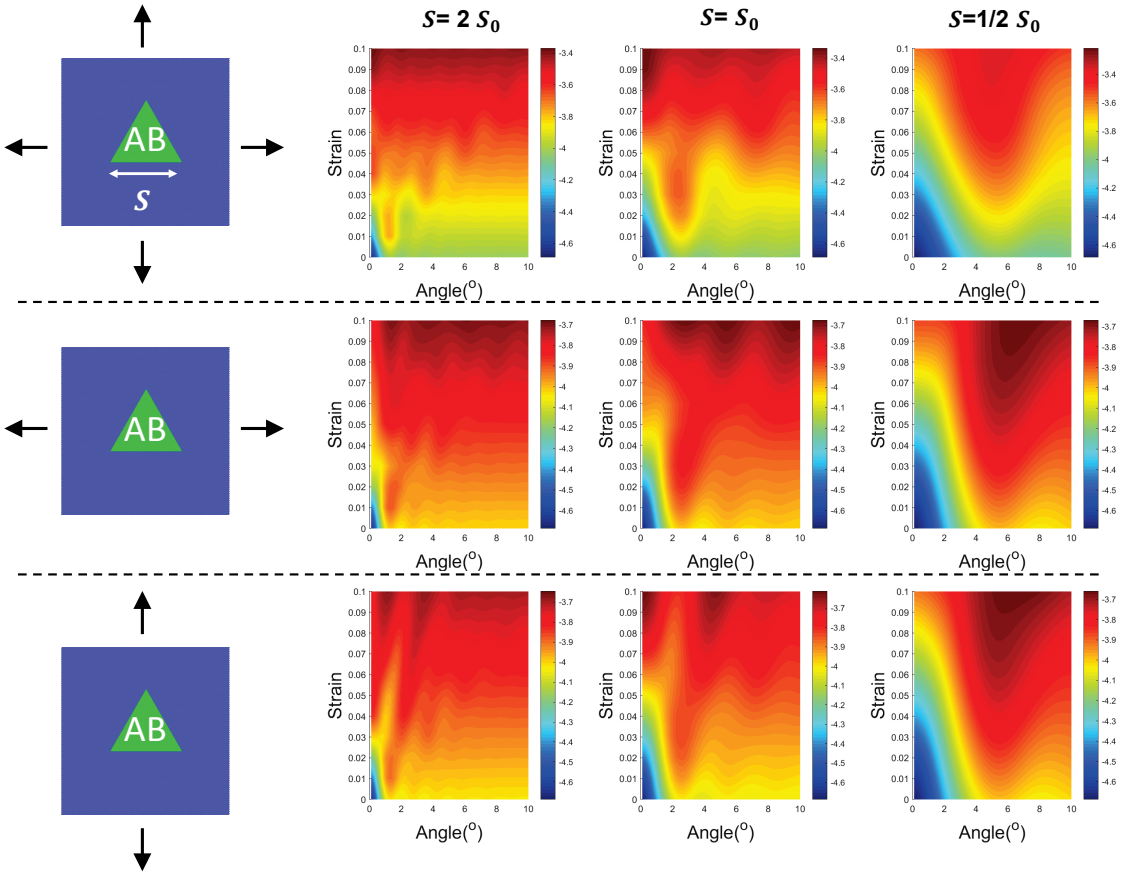


***Figure S10:*** *Energy maps in the space of strain and angle for three sizes. The top rows are for biaxial strain. The bottom two rows are for two uniaxial strain. The rotation center initial stacking is AB. Please note that this map is general for 2D material systems which share the same ratio of the triangular flake size to its lattice constant. See related discussion in main text.*

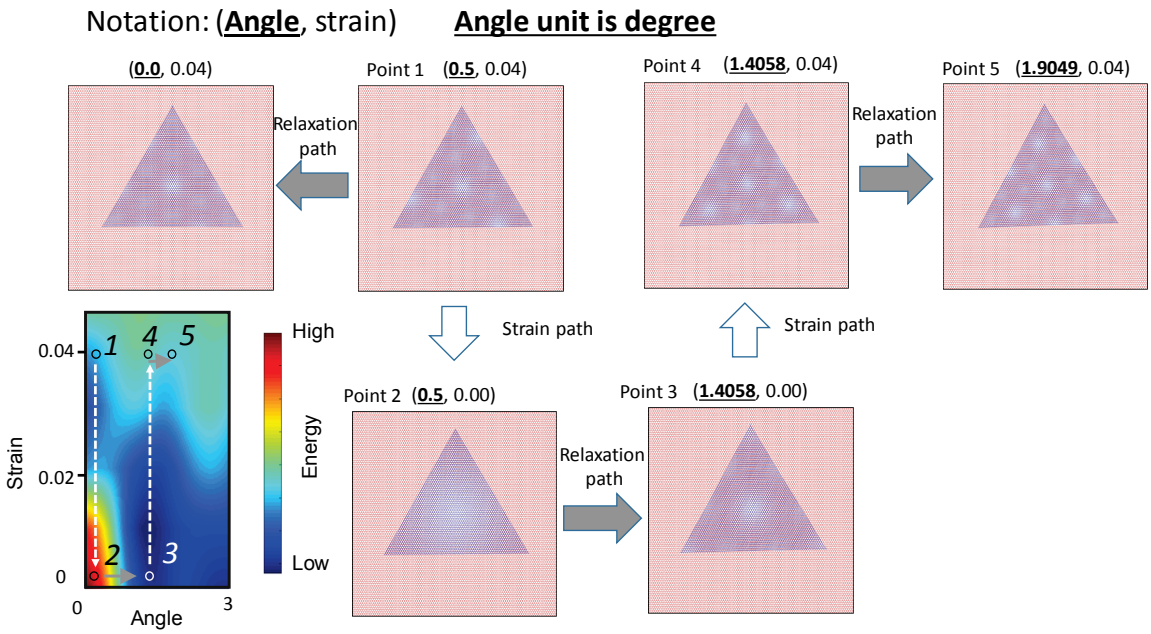


***Figure S11:*** *Demonstration of strain-controlled rotation of Figure 5(b) using bilayer graphene. The strain is biaxial. The white arrows denote the strain path. The grey arrows denote the relaxation path.*

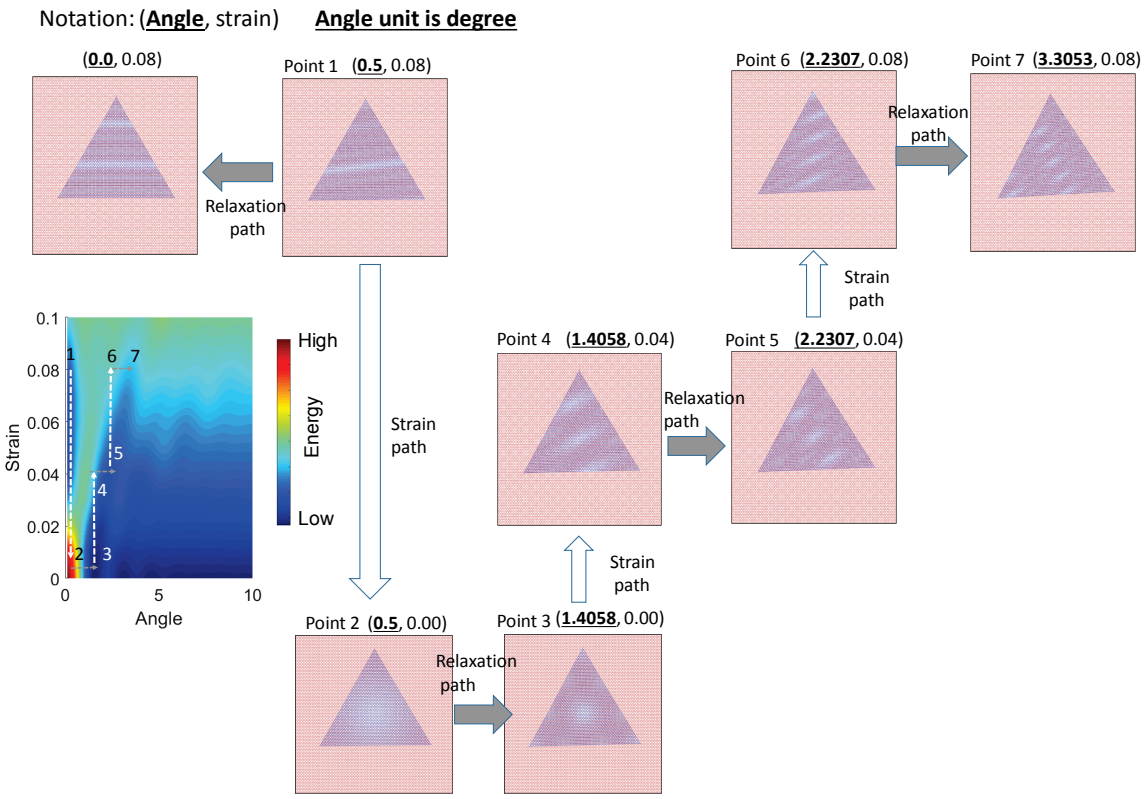


***Figure S12:*** *Demonstration of strain-controlled rotation of Figure 5(c) using bilayer graphene. The white arrows denote the strain path. The grey arrows denote the relaxation path.*

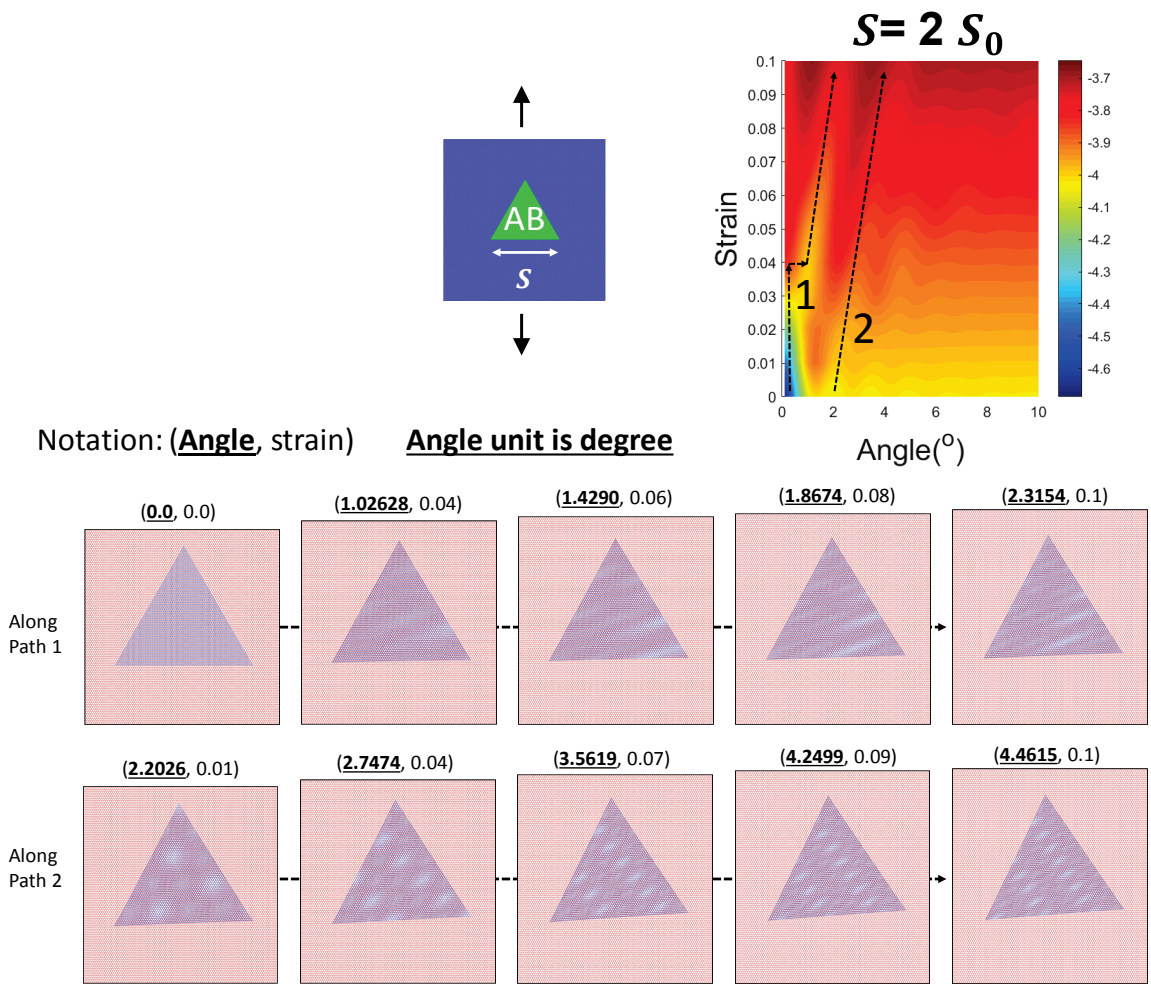


***Figure S13:*** *Demonstration of strain-controlled rotation using bilayer graphene according to the prediction in Figure S10 (rotation center initial stacking is AB; size of the triangle is $2S_0$; vertical loading). The black arrows in the energy map connect the energy relaxed state for small steps of increased strain. Two paths are shown with representative snapshots.*

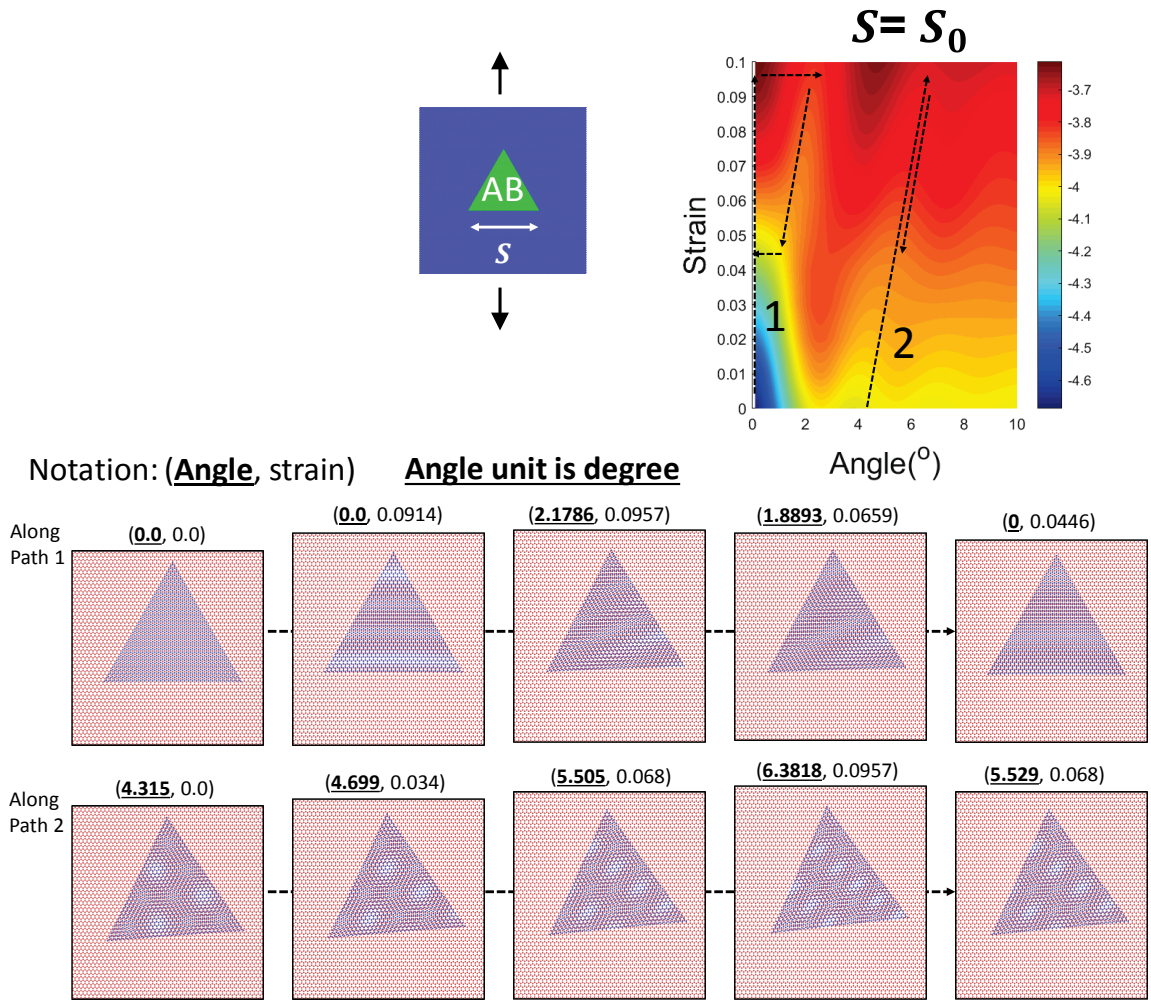


***Figure S14:*** *Demonstration of strain-controlled rotation using bilayer graphene according to the prediction in Figure S10 (rotation center initial stacking is AB; size of the triangle is $S_0$; vertical loading). The black arrows in the energy map connect the energy relaxed state for small steps of strain loading/unloading. Two paths are shown with representative snapshots.*

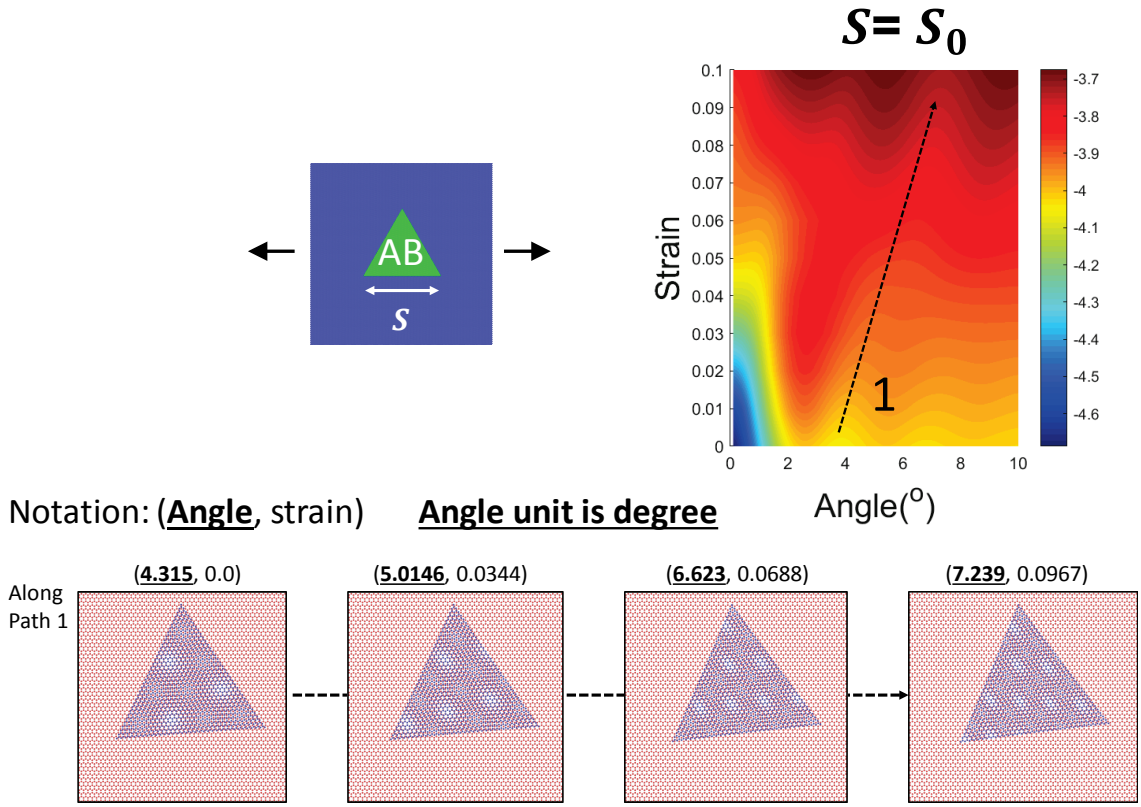


***Figure S15:*** *Demonstration of strain-controlled rotation using bilayer graphene according to the prediction in Figure S10 (rotation center initial stacking is AB; size of the triangle is $S_0$; horizontal loading). The black arrows in the energy map connect the energy relaxed state for small steps of strain loading/unloading. One path is shown with representative snapshots.*

## 8. Calculating of $MoSe_2$/graphene system with experimental comparison

We present a quantitative comparison with available experimental results in literature (Impact of a van der Waals interface on intrinsic and extrinsic defects in an $MoSe_2$ monolayer. Nanotechnology 2018, 29 (42). https://doi.org/10.1088/1361-6528/aad66f).

This experimental work investigates $MoSe_2$ grown on a graphene surface. The reported distribution of rotation angles for a triangular flake of $MoSe_2$ with side length of about 4 nm is shown in Figure S16 (c), and the calculated rotational energy landscape is shown in Figure S16 (b). We can see that there is an acceptable agreement between the predicted distributions of angles, noting that angles for which the energy is *high* are *not* favorable, so the experimental count is expected to be *low*.

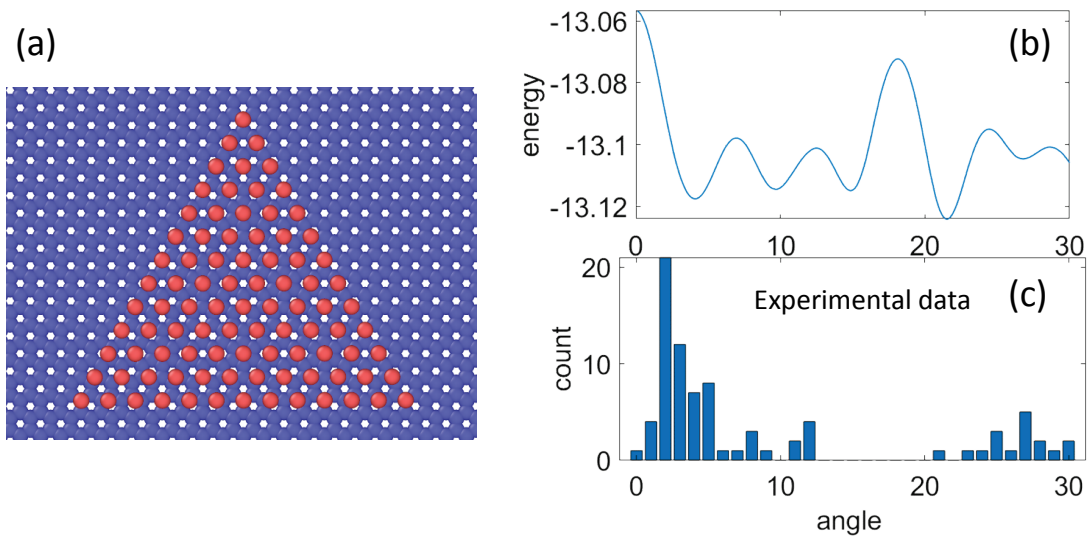


***Figure S16:*** *Imposing mismatch strain naturally extends to van der Waals hetero-layers, where the intrinsic lattice mismatch plays the role of strain. This figure is for its demonstration. (a) Top view of the interface lattice model for $MoSe_2$ on graphene system. A large lattice mismatch is present: the lattice constant of $MoSe_2$ is 0.328 nm, while the lattice constant of graphene is 0.246 nm. (b) The energy landscape calculated using ILM model. (c) The experimental characterized distribution of rotation angles for a system corresponding to the model in (a). The replotted data is taken from: Impact of a van der Waals interface on intrinsic and extrinsic defects in an $MoSe_2$ monolayer. Nanotechnology 2018, 29 (42). We can see that there is an acceptable agreement between the predicted distributions of angles: the region where energy is high is not favorable, so the experimental count is expected to be low.*

## 9. Evolving energy landscapes during growth

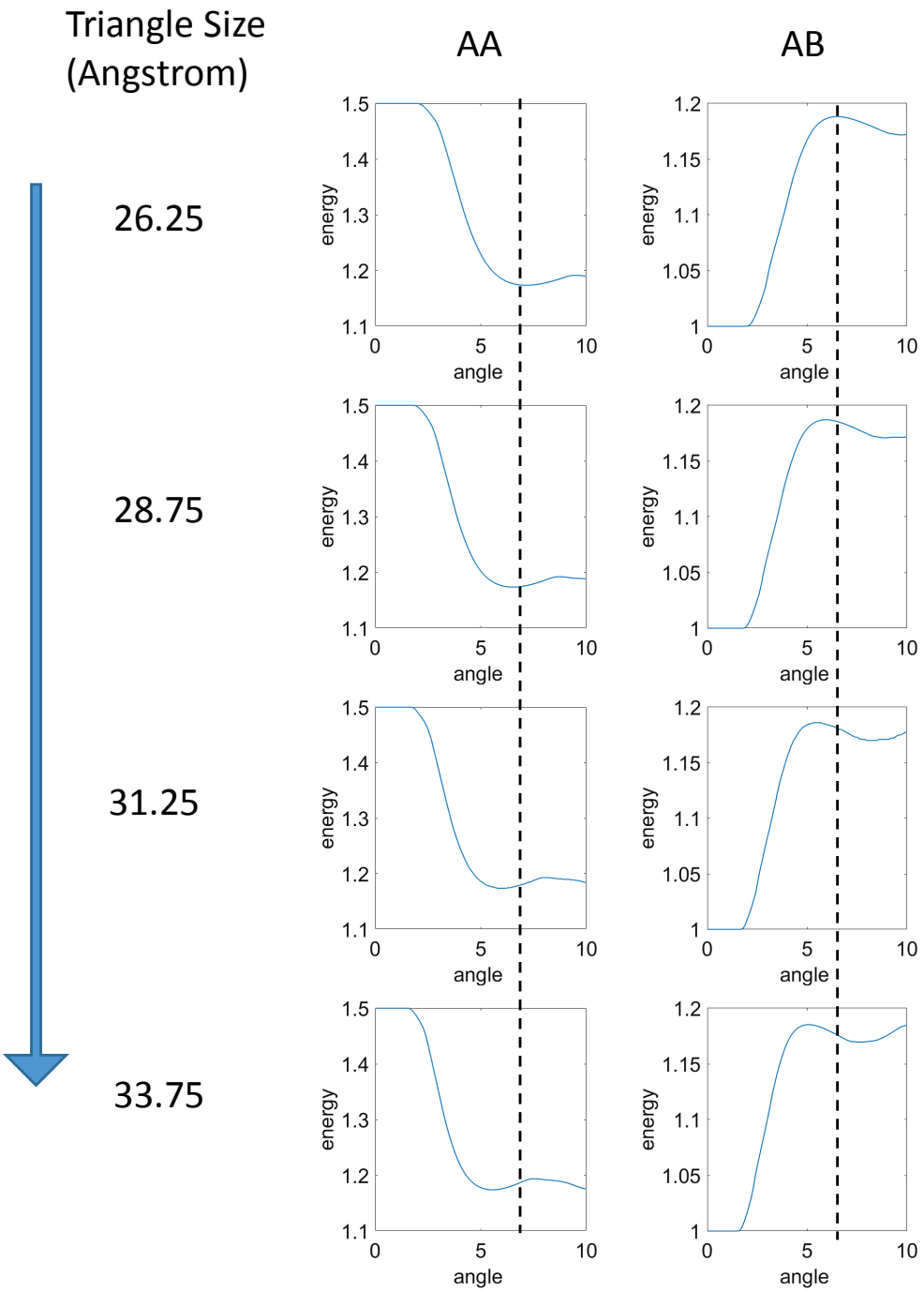


***Figure S17:*** *Comparison of energy-angle curves for a series of similar flake sizes of $MoS_2$, showing the shift in the energy landscape during growth. The triangle size is measured from the vertex of the triangle flake to its center.*